ORIGINAL PAPERS

Photodynamic therapy reduces cell viability, migration and triggers necroptosis in prostate tumor cells

Laura Calazans de Melo Gomes[1] · Amanda Branquinho de Oliveira Cunha[1] · Luiz Felipe Fernandes Peixoto[1] ·
Renata Graciele Zanon[2] · Françoise Vasconcelos Botelho[3] · Marcelo José Barbosa Silva[4] ·
Maria Etelvina Pinto-Fochi[5] · Rejane Maira Góes[6] · Flávia de Paoli[7] · Daniele Lisboa Ribeiro[1]

Abstract

Prostate cancer is the most common cancer in American men, aside from skin cancer. As an alternative cancer treatment, photodynamic laser therapy (PDT) can be used to induce cell death. We evaluated the PDT effect, using methylene blue as a photosensitizer, in human prostate tumor cells (PC3). PC3 were subjected to four different conditions: DMEM (control); laser treatment (L—660 nm, 100 mW, 100 J.cm^{-2}); methylene blue treatment (MB—25 µM, 30 min), and MB treatment followed by low-level red laser irradiation (MB-PDT). Groups were evaluated after 24 h. MB-PDT treatment reduced cell viability and migration. However, because MB-PDT did not significantly increase the levels of active caspase-3 and BCL-2, apoptosis was not the primary mode of cell death. MB-PDT, on the other hand, increased the acid compartment by 100% and the LC3 immunofluorescence (an autophagy marker) by 254%. Active MLKL level, a necroptosis marker, was higher in PC3 cells after MB-PDT treatment. Furthermore, MB-PDT resulted in oxidative stress due to a decrease in total antioxidant potential, catalase levels, and increased lipid peroxidation. According to these findings, MB-PDT therapy is effective at inducing oxidative stress and reducing PC3 cell viability. In such therapy, necroptosis is also an important mechanism of cell death triggered by autophagy.

Graphical Abstract
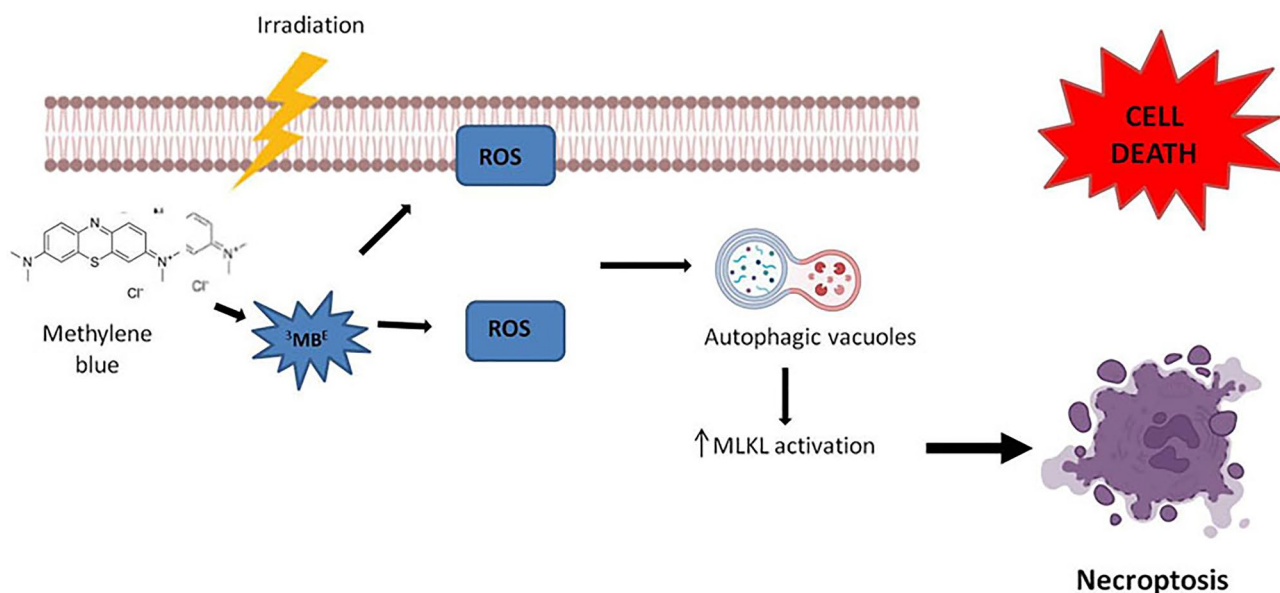
Extended author information available on the last page of the article

1 Introduction

According to the World Health Organization, in 2019, the life expectancy of the global population is 73.4 years on average [1]. It is evident that the trend of life expectancy is increasing; however, it has, as a direct consequence, a more significant occurrence of age-related diseases. Focusing on the male population, prostate pathologies are frequent during human aging. Given this, morphological and hormonal changes and prostate growth have been studied to understand the mechanisms behind prostate cancer, and are important to propose alternative solutions to prevent its incidence or efficient therapies. In addition, the International Agency for Research on Cancer [3] estimates that prostate cancer incidence will increase from 1,276,106 (2018) to 2,292,818 (2040) in the future. Prostate cancer and prostatic hyperplasia are the main disorders found in men above 50 years old and some factors may influence the progress of prostate carcinogeneses, such as chronic inflammation, metabolic syndromes, the individual's family history, and obesity. Additionally, dependence on androgen hormones and specific hormonal scenarios can initially favor this type of cancer and difficult the efficiency of treatments [3–5]. It is undeniable the last 50 years there were great advances in cancer therapies, mainly systemic therapies such as chemotherapy and immunotherapy. However, due to proliferation and plasticity abilities, tumor cells considered stemness gradually become resistant to treatments using different cellular mechanisms [6]. In this way, it is necessary to develop a continuum of new cancer-fighting therapies.

Photodynamic Therapy (PDT) has merged as a treatment to cause cell death only a century ago [7]. PDT is based on two non-toxic components that, when combined, produce cellular and tissue effects by a process that depends on oxygen. The first component is a non-toxic and light-sensitive dye called photosensitizer (PS) which consists of a molecule capable of transferring energy from light (photon) to molecular oxygen. The second component is the light at a specific wavelength to activate the PS. When PS is activated by light, an excited PS transfers its energy and it can induce superoxide anion ($O^{\bullet-}_2$), hydroxyl radical ($^{\bullet}OH$), and hydrogen peroxide (H_2O_2) production, in a reaction denominated type I. Reaction type II occurs when an excited PS transfer its energy inducing singlet oxygen ($^1O2$) production [8]. Both reactions occur simultaneously and depend on the type and concentration of PS, and oxygen availability. Then, reactive oxygen species (ROS) and the highly reactive radicals formed can react with cellular molecules such as endoplasmic reticulum, mitochondria, lysosome, and DNA, allowing a multimodal cell death [9]. Scientific research has focused on PDT applicability in tumor cells since advantages were observed when compared with conventional cancer treatments, including high selectivity, low toxicity, no drug resistance, tumor ablation, selective cancer destruction, and use with other therapies [10].

Methylene blue (MB) is a thiazine dye that presents excellent photochemical properties, being a potent photosensitizer for PDT. Once activated, MB generates high concentrations of singlet oxygen and ROS, causing oxidation of biomolecules and severe cellular cytotoxicity [11, 12]. Due to low-cost and commercial availability, MB has been used safely in different clinical practices for decades being an important dye, widely used in different fields of medicine [8]. In this context, a recent study reported that MB may be an inhibitor between SARS-CoV-2 spike protein and its cognate receptor ACE2 [13].

Regarding prostate cancer, there are few studies in the literature evaluating the use of PDT in cells in vitro and even fewer studies in vivo. Positive results of PDT-triggering cell death have been described in tumor cells, specifically in PC3 and LNCaP cells [14–16]. Concerning clinical application, vascular PDT (VTP) has gained prominence, which is a modality of therapy specialized in targeting blood vessels more than the tumor parenchyma. In this sense, molecules such as Palladium-bacteriopheophorbide, WST-09 and its water-soluble derivative WST-11 are currently the most widely studied agents used in localized prostate cancer VTP and have shown efficiency and promising results [17].

Although studies reveal the effectiveness of PDT in prostate cancer, different photosensitizers were used together with other chemical or thermal substances which consequently increases the cost of treatment. In this way, the present investigation explored cell death mechanisms of PDT methylene blue-based as an alternative cancer treatment to human prostate tumor cell (PC3), an aggressive and castration-resistant cell line.

2 Material and methods

2.1 Cell culture and treatments

Human prostate tumor epithelial cell line-PC3 was used in this investigation and maintained in DMEM medium supplemented with 10% fetal bovine serum (FBS) and 1% penicillin/streptomycin and kept in an incubator at 37 °C and 5% CO_2.

Methylene blue (MB) as a photosensitizer. To establish optimal concentration and non-toxicity effects for MB (Sigma Aldrich, USA), PC3 line cells were previously treated with different MB concentrations diluted in DMEM (from 0 to 50 μM), and the dose–response curve was evaluated. PC3 cells were incubated for 30 min at 37 °C and, and

afterward, they were washed with PBS and supplemented with DMEM medium prior to low-level laser irradiation. Thereby, an MB concentration of 25 µm (MB group) was used for all experiments.

Low-level laser. A therapeutic low-power red laser (Photon Lase III, AsGaAl—D.M.C. Equipamentos Ltda, São Paulo, Brazil) was used for experimental procedures. Laser physical parameters are described in Table 1. PC3 cells were grown in 96-well, 6-well plates or flasks and received laser irradiation. Space among wells was maintained to avoid overlapping irradiations. Red laser irradiation was applied at one point perpendicularly above the culture plates (LASER group). Immediately after MB incubation, DMEM was replaced, and PC3 cells were irradiated as described above (MB-PDT group). Finally, the control group received only DMEM medium supplemented for the same experimental period. Cells were evaluated 24 h after treatments.

2.2 Cell proliferation assay by MTT

PC3 cell viability was evaluated after treatments using an MTT-based cell titer 96 Aqueous Non-Radioactive Cell Proliferation Assay kit (MTT G4000, Promega, Madison, WI), which contains the compound [3-(4,5- dimethylthiazol-2yl)-2,5-diphenyltetrazolium bromide]-MTT. Briefly, cells were grown in flat-bottomed 96-well plates at a 15×10^3/per well concentration. After the experimental period, cells were treated with MTT according to the manufacturer's instructions. Formazan compound intensity, a product resulting from MTT reduction after its reaction with active mitochondria of living cells, was quantified by the absorbance at a wavelength of 570 nm. The absorbance is directly proportional to the number of live cells present in the culture. Three repetitions of the experiment were performed, containing samples in triplicate. To confirm autophagy cell death, proliferation was also evaluated by MTT in cells treated with autophagy inhibitor (chloroquine—5 µM diluted in DMEM) before and after MB-PDT.

Table 1 Laser physical parameters

Wavelength (nm)	660
Diode laser	AsGaAl
Power (mW)	100
Light emission mode	Continuous
Spot area (cm^2)	0.028
Energy per point (mJ)	2.8
Energy density ($J.cm^{-2}$)	100
Time per point (s)	28
Number of points	1
Application technique	Punctual
Number of treatment sessions	One

2.3 Cell migration/cell scratch assay

PC3 cell ability to migrate under the appropriate treatments was evaluated using a cell scratch/wound healing assay. Therefore, the cells were grown in 12-well plates (4 wells per group) and kept in an incubator until they reached close to complete confluence. With a 100 µL tip, a scratch was performed at the bottom of wells in a cross-section to remove cells. Then, cells were treated and photographed immediately (0 h), 24 h, and 48 h after treatments. Five regions of the same well were documented using a $10 \times$ microscope objective for each exposure time. Subsequently, images were analyzed by TScratch software [18] which measures the distance of the scratched area over time. The closure of the scratched area represents migratory cells movement from the border to the center of the scratch.

2.4 Immunofluorescence assay for Bcl-2 and LC3

The immunocytochemistry assay evaluated the Bcl-2 expression (apoptosis resistance-related) and LC3 (autophagy marker). Thus, PC3 cells were treated in 6-well plates containing a coverslip at the bottom for cell adhesion. Cells were fixed in 4% methanol for 20 min, washed in TBS-T buffer, and blocked for nonspecific interactions with 3% albumin for 1 h. Then, primary antibodies Rabbit anti-Bcl-2 (Cell Signaling #3498, Massachusetts, USA) and Mouse Anti-LC3 B (Cell Signaling #43,566, LC3 type I and II) (1:500 in 3% albumin) were incubated at 4 °C overnight. After washes, cells were incubated in Texas Red conjugated secondary antibody (Jackson Laboratory, Maine USA) (1:1000 in 3% albumin) for 1 h at room temperature. Then, cells were washed and treated with YO-PRO-1 (for BCL-2 reaction, #Y3603) and TO-PRO-3 (for LC3 reaction, #T3605) (Thermo Scientific, Massachusetts, USA) for nuclei counterstaining and mounted on slides using glycerol. Immunoreaction was analyzed using a confocal microscope (LSM 510 Meta; ZEISS, Oberkocher, Germany), 10 different microscopic fields/slides; 3 slides per group, totaling 30 analyzed areas/group. Positive cells were quantified by fluorescence intensity analysis (normalized by the cell number in each image) using the ImageJ program [19].

2.5 Evaluation of active caspase-3

Active caspase-3 quantification was performed in PC3 cells using EnzChek® Caspase-3 Assay Kit #1 *Z-DEVD–AMC Substrate (#E13183, Thermo Scientific Massachusetts, USA) following the manufacturer's instructions. Briefly, PC3 cells were grown in 12-well plates at 1×10^6/well density, and they were trypsinized after 24 h of treatment. Cell pellet obtained from each sample was resuspended in 50 µL of cell lysis buffer and incubated for 30 min at 4 °C. Then,

the buffer-diluted Z-DEVD-AMC substrate was added to each sample in a dark 96-well plate and incubated for 30 min at room temperature. At the end of the reaction, active caspase-3 levels were measured by microplate fluorimeter (excitation/emission ~ 342/441 nm). The fluorescence is a direct measurement of the active caspase-3 amount on AMC standard curve. The fluorescence value for each sample was normalized by the protein concentration of the respective sample. Two repetitions of the assay were performed, with readings in triplicate for each group.

2.6 Flow cytometry

PE Annexin-V Apoptosis Detection kit (#559,763, BD Biosciences, New Jersey, USA) was used to determine apoptosis/necrosis, according to the manufacturer's instructions. 1×10^6 cells were used for flow cytometry, and after 24 h of treatments, PC3 cells were collected, transferred to microtubes, and centrifuged (1500 rpm for 5 min). The cell pellet was washed in PBS and resuspended in 100 μl of $1 \times$ Annexin binding buffer. Then, 5 μL of Annexin V and 7-AAD were added to all samples. After 15 min of incubation, 400 μL of binding buffer was added to all samples, and the reaction was analyzed by flow cytometry in appropriate fluorescence channels (Annexin PE ~ 575 nm—orange; 7-AAD ~ 650 nm- red). Cytometry controls: cells labeled only with Annexin; cells labeled only with 7-AAD, and cells without labeling. Sample cells labeled only with 7-AAD were previously permeabilized with 3% formalin for 30 min. The experiment was carried out in triplicate for each group.

2.7 Quantification of acid vesicles by acridine orange staining

Acridine orange (AO) is a dye with cationic properties, and it can be accumulated in acidic cell compartments, emitting bright red fluorescence (640 nm) [20]. Thus, acid vesicle quantification can provide data about autophagy. To quantify cytoplasmic acid vesicles, PC3 cells were grown in 6-well plates containing a coverslip for cell adhesion at the bottom. Then, 24 h after treatments, cells were washed with PBS and stained with AO (5 μg/mL, Sigma Aldrich, USA) for 10 min in the dark. After the washing step, live cells were visualized using an inverted confocal microscope (LSM 510 Meta; Zeiss, Oberkocher, Germany). AO-stained vesicle fluorescence was detected using a filter that provides an excitation band pass (BP) of 450–490 nm with an emission long pass (LP) of 515 nm. Red label quantification was performed by ImageJ software [15], using 10 different images/slides; 3 slides/group captured in 40 × objective. Red fluorescence intensity was normalized by the number of cells in each image.

2.8 Oxidative stress evaluation

After different treatments of PC3 cells, they were treated with RIPA- radio-immunoprecipitation assay buffer for 30 min for protein extraction, followed by centrifugation at 14,000 rpm for 20 min at 4 °C. The supernatant was collected and the total protein content in samples was determined by the Bradford method [21].

– Catalase activity was quantified at 240 nm by the decomposition of 1 μM of H_2O_2 per minute, according to the method of Aebi [22].
– Total antioxidant activity was evaluated by ferric reduction (Fe^{3+}/Fe^{2+}) at low pH, forming the ferric-tripyridyl-triazine complex (TPZP) which has an intense blue color and can be monitored at 593 nm [23]. The reagents used include: acetate buffer (300 mM/L^{-1}, pH 3.6); 10 mM/L^{-1} TPTZ in 40 mM/L^{-1} HCl; 20 mM $FeCl_3.6H_2O$ in distilled water. FRAP working solution: 25 mL acetate buffer, 2.5 mL TPTZ solution, and 2.5 mL $FeCl_3$ solution. Ten microliters of the sample, 25 μL of water, and 25 μL of working solution were added to a microplate and incubated for 6 min at 37 °C. The absorbance was measured in a spectrophotometer at 593 nm (Molecular Devices, Menlo Park, CA, USA). The total antioxidant activity was measured based on a calibration curve of 1000, 800, 400, 200, 100, and 50 μM Trolox. All solutions used were freshly made.
– The malondialdehyde (MDA) level, an indicator of free radicals generated by lipid peroxidation, was estimated using the double heating method of Draper and Hadley [24]. A 100 μL aliquot of the cell medium was used as a sample. Then, 300 μL of 0.4% thiobarbituric acid solution diluted in 0.2 M HCl was added to the samples and incubated for 60 min at 90 °C. Subsequently, the colored derivative of the MDA–TBA complex (TBARs) was extracted with n-butanol followed by centrifugation and quantification at 532 nm. The data were expressed as nmol/μL TBARs.
– Quantification of reduced glutathione: Protein content of the samples was precipitated with 20% trichloroacetic acid (TCA), centrifuged for 6 min, 10,000 g at 4 °C, and the supernatants were used to measure reduced glutathione (GSH). To determine the GSH concentration, 100 μL of samples were mixed with 120 μL, 0.5 M phosphate buffer (pH 7.4 with 5 mM EDTA), 350 μL of distilled water, and 30 μL of 2 mM 5.5'-dithiobis-2-nitrobenzoic acid (DTNB). The GSH of samples reacts with DNTB, producing 5-to-2-nitrobenzoic acid (TNB), which can be read at 412 nm in the spectrophotometer. For the calculations, it was subtracted the blank from the absorbance of the samples and used the molar absorptivity coefficient (TNB) of 13.6 mM-1 cm-1(412

TNB = 13.6) to determine the concentration of reduced glutathione, according to Akerboom and Sies., 1981 [25].

2.9 Western blotting

PC3 cells were seeded in 6-well plates and treated as described above. Each treatment was performed in three repetitions. After treatment, protein content was extracted with RIPA buffer (R0278, Sigma Aldrich) containing protease inhibitors (Protease Inhibitor Cocktail—Sigma Aldrich) 0.1 mM sodium orthovanadate, 100 mM PSMF; cells were scraped and then harvested. After 10 min of shaking at 4 °C, samples were centrifuged (14,000 rpm, 15 min, 4 °C), and protein content was quantified by the Bradford method [21]. Subsequently, aliquots containing 10 µg of protein were separated by SDS-PAGE on 10% polyacrylamide TRIS–glycine gel and after electrophoresis, electroblotted upon nitrocellulose membranes. Nonspecific protein-binding sites were blocked with 5% albumin diluted in 0.2% TBST for 60 min at room temperature. Membranes were subsequently incubated overnight at 4 °C with rabbit anti-phospho-MLKL (#37,333, Cell Signaling Technology) and rabbit anti-β-actin (sc-130656, 1:1000) diluted 1:800 and 1:500 in 3% albumin in TBST, respectively. Subsequently, membranes were incubated with anti-rabbit HRP-conjugated IgG diluted 1:5000 in TBST (3% albumin) for 1 h. The immunoreactive components were detected by the ECL detection kit (GE Healthcare) and the chemiluminescence was analyzed using Amersham Imager 600 (GE Healthcare Life Sciences). Protein band densitometry was performed by Image J software [19], and densitometric values of p-MLKL were normalized with β-actin.

2.9.1 Statistical analysis

All data were first checked with the Kolmogorov–Smirnov test. Then, normal distribution data were analyzed by ANOVA followed by Tukey's test (parametric test) for multiple comparisons. At the same time, non-normal distribution data were analyzed by a non-parametric test, ANOVA followed by Kruskal–Wallis test. All statistical evaluations were performed using the Instant GraphPad software.

3 Results

3.1 PDT can reduce cell migration and viability

PC3 cell viability was assessed by MTT assay (Fig. 1). A dose–response experiment was performed preliminarily to choose MB dosage to be used in this investigation. The dose–response curve showed that MB has a dark cytotoxic effect at doses higher than 30 µM (Fig. 1a). Regarding PDT, there was a significant reduction in cell viability at all MB dosages. However, the most notable cytotoxicity effect of PDT could be noted at doses of 30, 40, and 50 µM MB (Fig. 1a). Thus, 25 µM MB dosage was chosen for the treatments performed in this study.

MTT in Fig. 1b demonstrated that 25 µM MB was able to reduce cells in MB-PDT and MB groups compared with the control ($p < 0.05$) while the laser group did not show significant changes. In addition, when autophagy is inhibited by chloroquine, PC3 cell viability unexpectedly is not restored in MB-PDT.

PC3 cells migratory activity was decreased after 24 and 48 h for both treatments (MB and MB-PDT) compared with the control group. However, cell migration was further reduced in the MB-PDT group, which still maintained about 5% of the scratch area compared to the other groups that practically closed the scratch area after 48 h (Figs. 2a and b), especially the laser group.

3.2 Cell viability decreased by MB-PDT is not mainly triggered by apoptosis

Apoptosis was evaluated by active caspase-3 levels quantification in samples after treatments. Although it was observed a trend in caspase-3 activation by MB-PDT, there was no statistical difference compared with the control group (Fig. 3a). Apoptotic and necrotic cell populations were further studied by flow cytometry. Although the statistical difference was not found, a higher number of apoptotic cells in MB and MB-PDT groups was observed when compared with the control (Figs. 3b and c). Regarding necrosis, this kind of cell death represented less than 1% in all groups (Figs. 3b and c). Additionally, Bcl-2 immunofluorescence results showed that all treatments did not change Bcl-2 levels, which is a protein directly associated with apoptosis resistance (Fig. 4).

3.3 MB-PDT increases acidic compartments and LC3 may lead to autophagy

Considering that MB-PDT did not alter PC3 cells apoptotic activity, autophagy was investigated as a possible cell death mechanism to explain cell viability reduction caused by such treatment. According to AO quantification, there was a significant increase in the acidic compartment (which mainly represents autophagic vacuoles and lysosomes) only in cells treated with MB-PDT when compared with the control group (Figs. 5a and b). Furthermore, LC3 puncta immunofluorescence, an important monitor of autophagic activity, was also evaluated. MB-PDT group also presented a significant increase in LC3 content compared with the

Fig. 1 Phototoxic effect of MB-PDT in PC3 cells. a-Dose–response curve of PC3 cells 24 h after treatment with different MB concentrations and/or PDT irradiation. Dark cytotoxicity was found at MB concentrations greater than 30 μM. The cytotoxic effect of MB was potentiated by PDT. b-MTT performed with a dose of 25 μM MB shows a significant reduction in cell viability after MB-PDT treatment. Cells were treated with MB and maintained in the dark (MB) or exposed to a low-level laser at 100 J.cm^{-2} energy density (MB-PDT) for 24 h. L group was only irradiated by low-level laser, and the control group was maintained without treatment. MTT was also performed in a cell group treated with chloroquine before MB-PDT treatment (MB-PDT + CLQ). There was no restoration of cell viability with autophagy inhibition. Results are expressed as fold change relative to control and represent the mean ± SD of three different experiments. *p < 0.05 Statistical difference in comparison to control
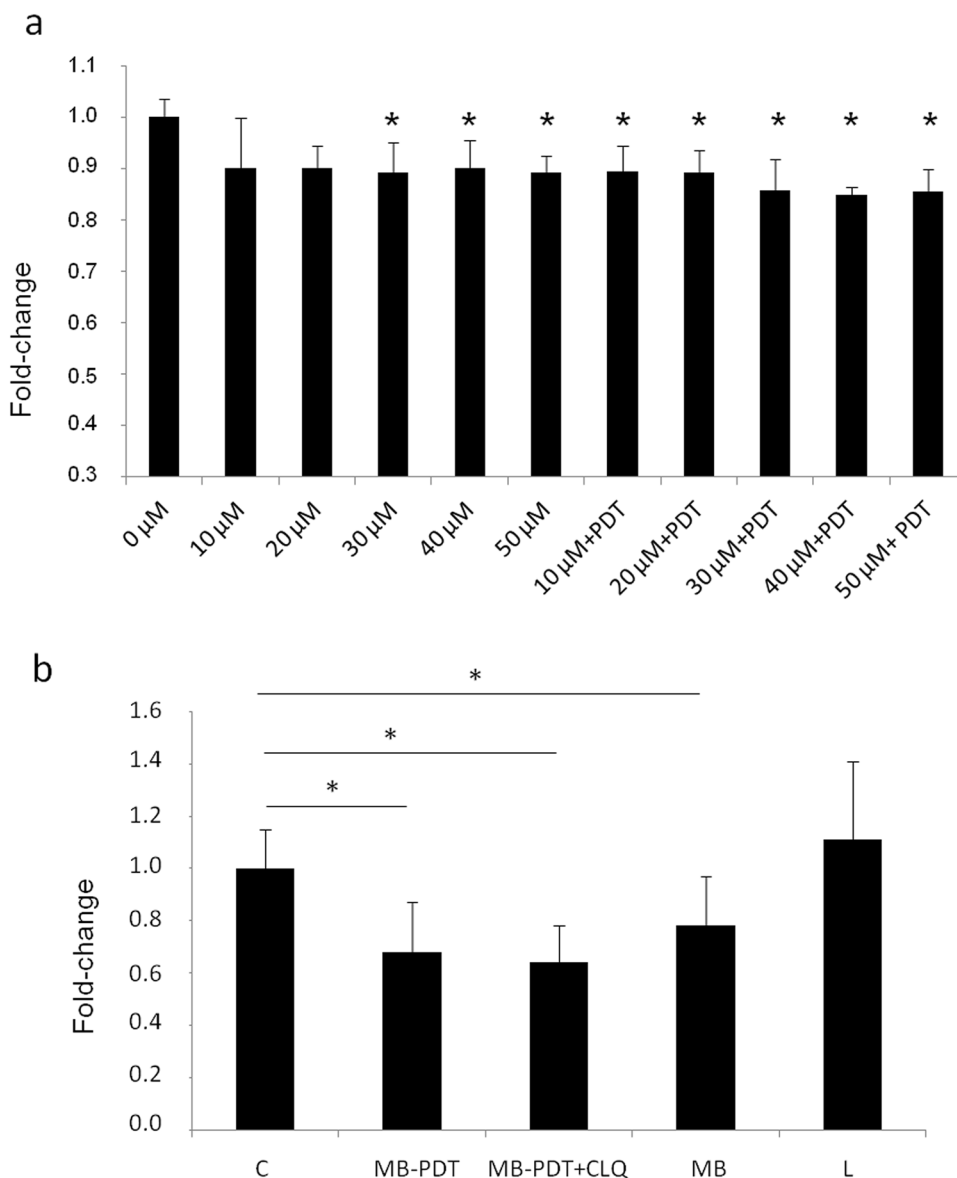
control (Figs. 6a and b). When chloroquine, an inhibitor of autophagy was used before and after MB-PDT, the levels of acid compartments and LC3 were restored. Such findings suggested that autophagy could be triggered by MB-PDT in these cancer cells (Figs. 5 and 6).

### 3.4 Necroptosis is also involved in MB-PDT-induced cell death

Another cell death mechanism, necroptosis, was analyzed by quantifying MLKL protein content in PC3 after MB-PDT treatments. Western blotting analysis showed that MB-PDT therapy increased the levels of phospho-MLKL in PC3 cells in comparison to the control group. (Figs. 7a and b). Although the laser group has also presented elevated activation of MLKL, such a cell death mechanism was

potentiated by photosensitizer association once it was higher in MB-PDT.

3.5 MB-PDT reduces antioxidant activity and leads to higher lipidic peroxidation

Adaptive response to oxidative stress was analyzed by intracellular levels of antioxidant enzymes, total antioxidant activity, and products generated by oxidative stress (Fig. 8). MB-PDT led to a 75% decrease in catalase levels and a considerable reduction in total antioxidant activity in PC3 cells (Figs. 8a and b). GSH levels did not reach statistical significance in any treated group (Fig. 8c). This lower antioxidant potential caused by MB-PDT was associated with higher production of MDA in PC3 cells, as it can be seen as a tenfold increase in TBARS test (Fig. 8d). MDA production directly indicates lipid peroxidation

Fig. 2 MB-PDT reduced Cell Migration in PC3 cells. **a** Wound healing/Cell Scratch Assay shows reduced migration activity in PC3 cells treated with MB-PDT. Cells were submitted to this assay after incubation with 25 µM MB and maintained in the dark (MB) or exposed to a low-level laser at 100 J.cm^{-2} energy density (MB-PDT). L group was only irradiated by low-level laser, and the control group was maintained without treatment. Microscopic images were captured at times 0, 24, and 48 h after treatments. **b** Graphical representation shows the absolute area of scratch, and the difference between time 48 h (black bars) and 0 (gray bars) represents the migration area. Results represent the mean ± SEM of three different experiments. *Statistical difference in comparison to control; a b, c comparison between different exposure times of the same group. Scale Bar: 1000 µm
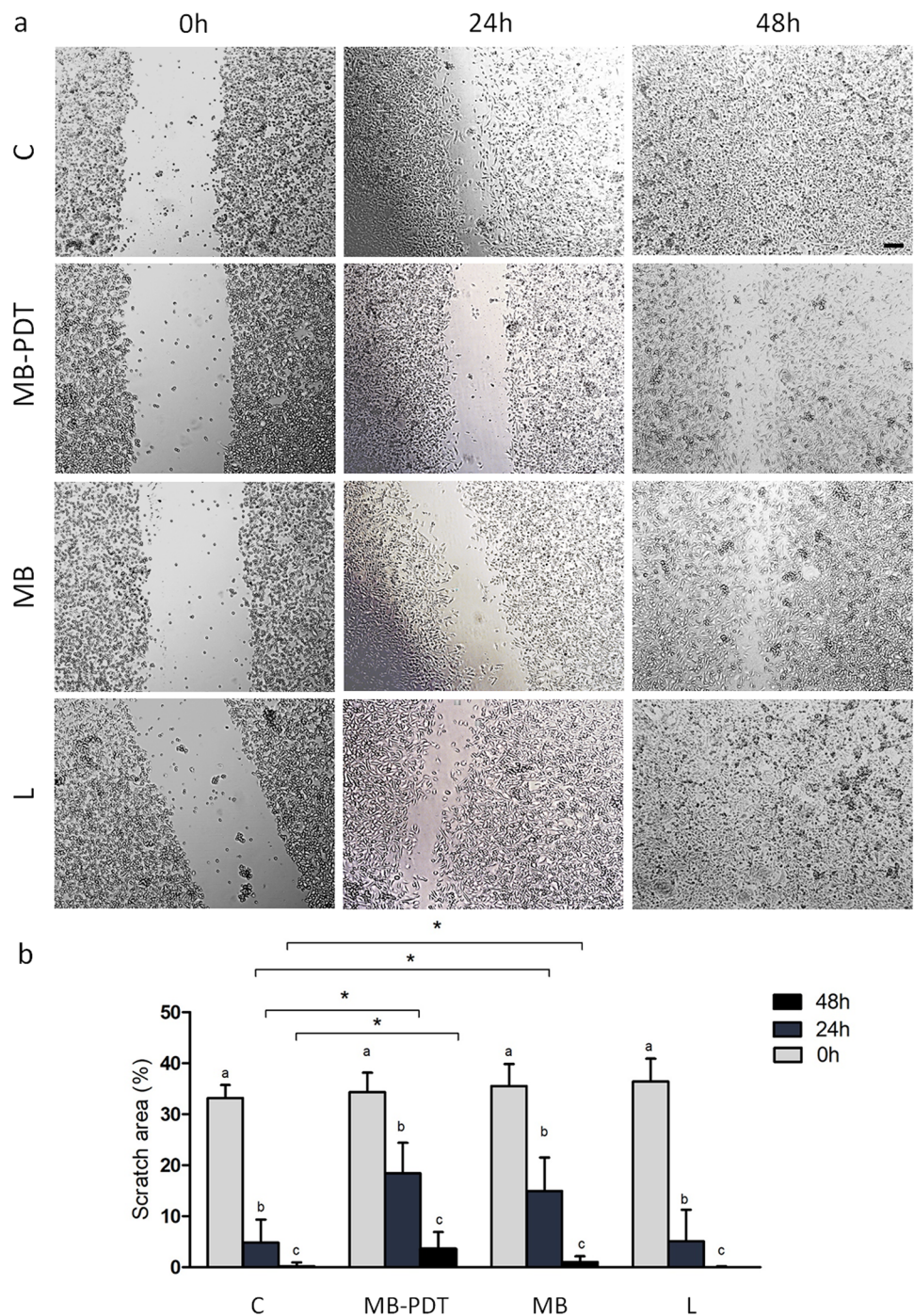
and cellular damage caused by oxidative stress. Interestingly, laser and MB treatments alone also affected enzyme levels and antioxidant activity in PC3 cells significantly, indicating that such effects observed for MB-PDT group are not exclusive to the combined treatment but may potentiate oxidative damage.

Fig. 3 Photoxicity of MB-PDT is not related only to Apoptosis. **a** Active caspase-3 levels quantification in PC3 cells after incubation with 25 μM MB and maintained in the dark (MB) or exposed to low-level laser at 100 J.cm^{-2} energy density (MB-PDT). L group was only irradiated by low-level laser, and the control group was maintained without treatment. The results are expressed as fluorescence relative to protein concentration (mean ± SD, $n = 3$). **b** and **c** Annexin V/ 7AA binding and measured by flow cytometry to detect apoptosis/necrosis cell death. *$p < 0.05$ in comparison to the control
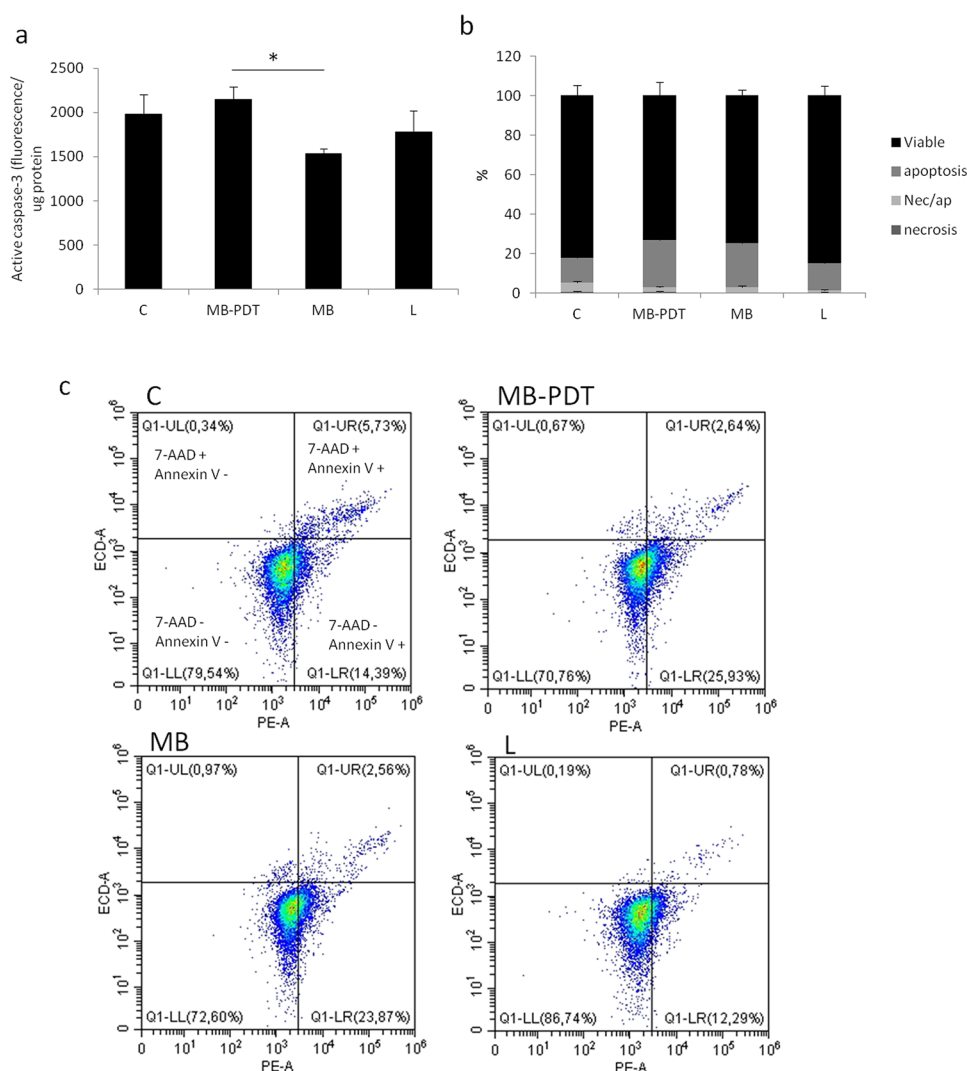
4 Discussion

PDT knowledge goes back to the beginning of the twentieth century when it was demonstrated the use of PDT in cancer treatment using experimental animal models, and later on, the effectiveness of PDT for human cancer was confirmed, and different photosensitizers have been then proposed [26]. MB is a cheap and common dye used in medical and dentistry applications, presenting phototoxic properties and being a potential photosensitizer for PDT. Since MB has already been approved in humans for different treatments, such as malaria, and it presents photosensitizing potential, it is surprising it has not been investigated as a front-line agent in prostate cancer PDT yet [8, 12, 27]. In this work, it was evaluated the cytotoxic effect of MB-PDT in a very aggressive prostate cancer cell line (PC3) as well as the mechanism of cell death related to such therapy.

Some researchers in different tumor cells have already described the cytotoxic potential of PDT associated with methylene blue. Bellin and other authors [28] observed decreased viability of 6C3HED cells. Moreover, the cytotoxicity of MB-PDT therapy has also been demonstrated in other cell lines, including breast cancer cells [29, 30], lung [31], and HeLa cells [32], among others. However, this is the first study involving such photosensitizer in prostate tumor cells and it can confirm MB capacity of decreasing the viability of PC3, bringing new perspectives to prostate cancer treatment.

The photosensitizer dose should be as low as possible to not cause dark cytotoxicity but high enough to cause PDT phototoxicity. Our previous studies (data not presented) showed that MB could not reduce the viability of the PC3 cells at doses below 25 μM, and therefore, this concentration was chosen. Several studies involving MB as a photosensitizer do not show dark cytotoxic effects, but most used lower concentrations than ours. Thus, considering the dark cytotoxicity found in our investigation, we believe that an adjustment in the MB treatment may improve the outcome

Fig. 4 Immunofluorescence for Bcl-2 (**a**) and quantification (**b**) in prostate epithelial tumor cells-PC3 after incubation with 25 μM MB and maintained in the dark (MB) or exposed to low-level laser at 100 J.cm^{-2} energy density (MB-PDT). L group was only irradiated by low-level laser, and the control group was maintained without treatment. *$p < 0.05$ Statistical difference between treated groups and control. All values are represented as the means ± SD of three experiments
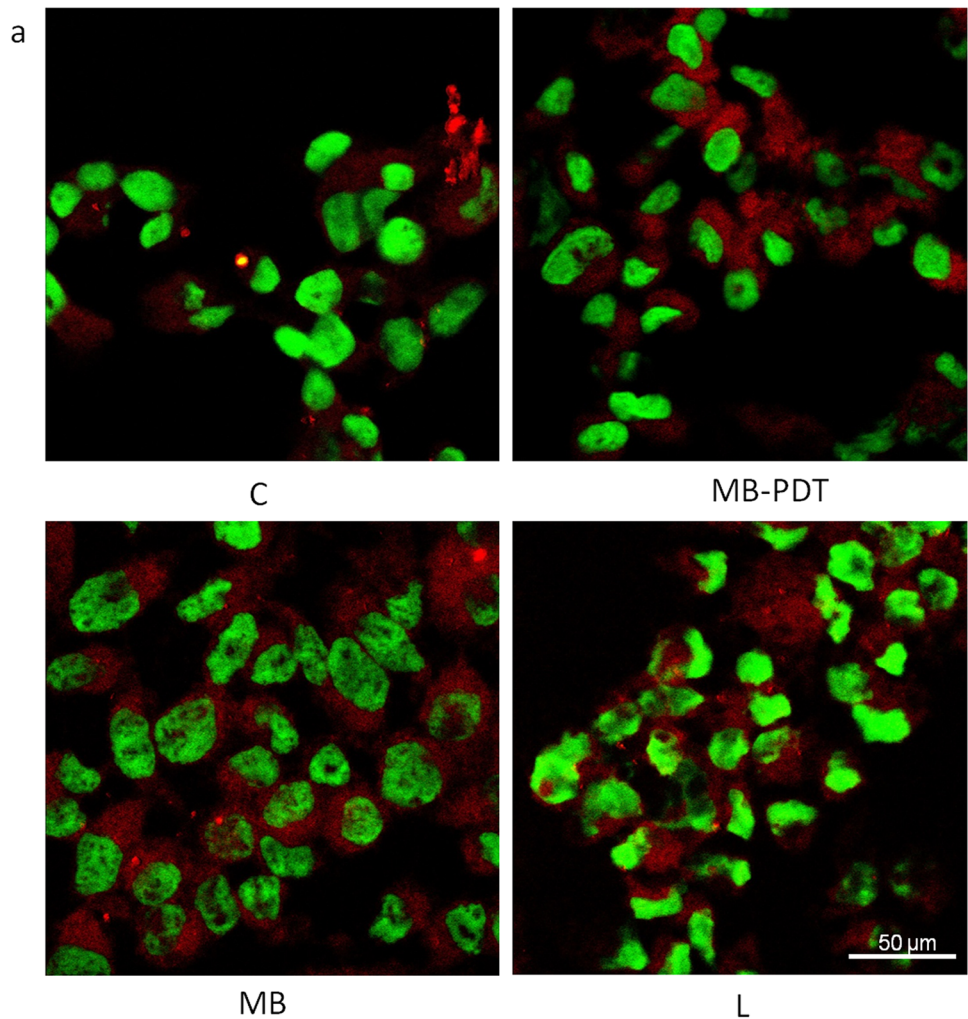

of this PDT protocol, including incubation time. Although some investigations pointed to therapy efficiency, they also show reduced cell viability after MB treatment without association with laser irradiation. A reduction of about 60% (THP1 macrophages) and 78% (MCF-7 cells) in cell viability using MB treatment at 20 and 25 μM, respectively, was already reported [33, 34]. In addition, Ma and other authors [35], 2020 also demonstrated the dark cytotoxic effect of MB in concentrations above 10 μg.ml^{-1} in SiHa cells, a dose similar to ours.

This investigation showed that MB-PDT decreased the PC3 cells migratory capacity. PC3 cells originated

Fig. 5 Representative images of acidic compartments by acridine orange fluorescence **a** in prostate epithelial tumor cells -PC3 after incubation with 25 µM MB and maintained in the dark (MB) or exposed to low-level laser at 100 J.cm^{-2} energy density (MB-PDT). L group was only irradiated by low-level laser, and the control group was maintained without treatment. **b** The quantification of acridine orange fluorescence shows increased levels of acidic compartments in MB-PDT levels and its reduction after autophagy inhibition by chloroquine (CLQ+ MB-PDT). All values are represented as the means ± SD of three experiments. *$p < 0.05$ compared to control; a $= p < 0.05$ compared to MB-PDT
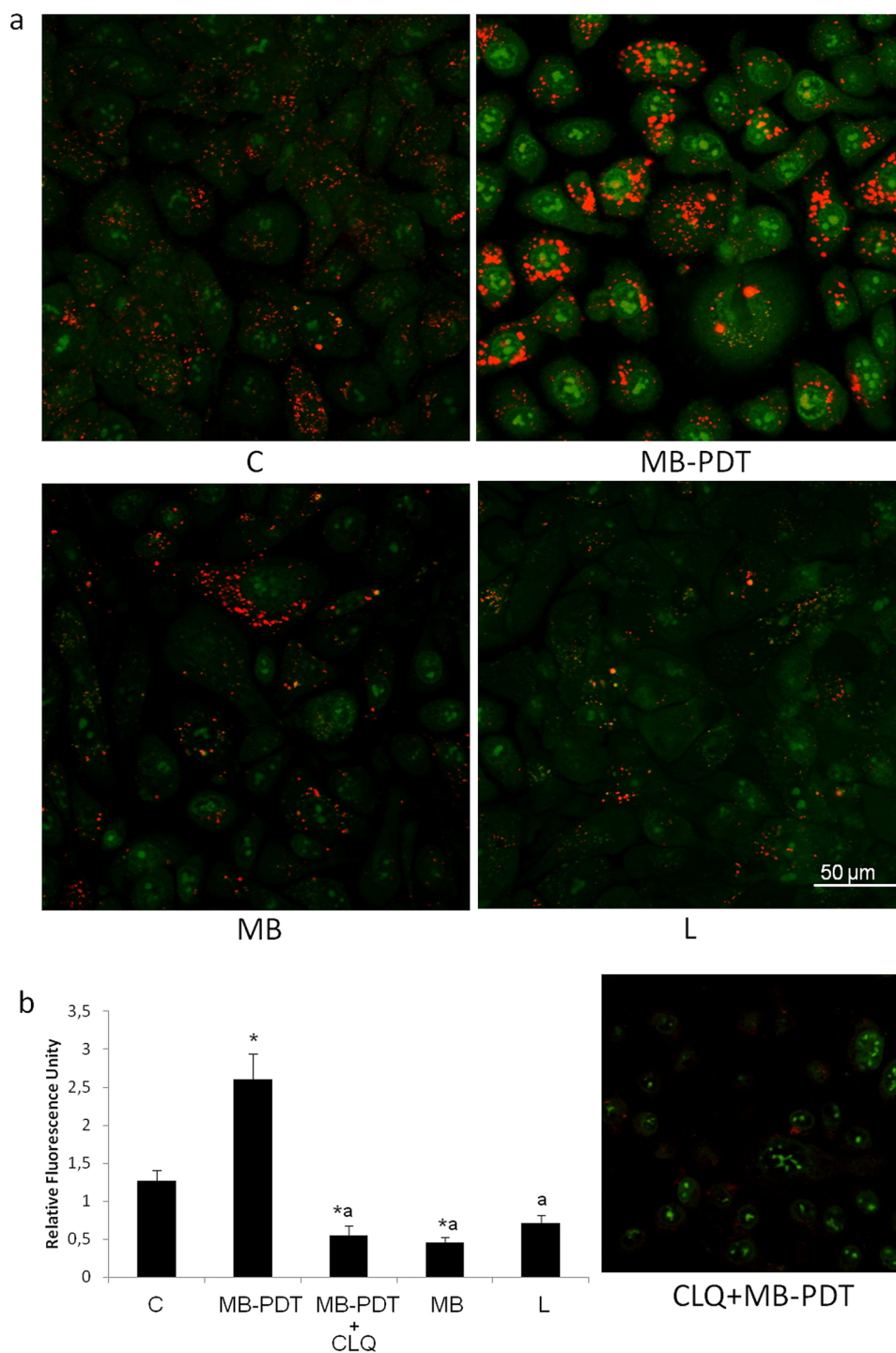

from metastatic tumors are resistant to androgen ablation and have highly aggressive phenotypes, challenging to treat. The potential of tumor cells to generate metastases is closely related to the cells acquiring phenotypes that give them migratory properties, and it is one of the great challenges for cancer therapies [36]. The reduction in migratory capacity caused by MB-PDT may be seen as an important result in association with cytotoxicity and can be allied to other traditional therapy.

In general, cell death mechanisms described in PDT are apoptosis, necrosis, and autophagy, being the same photosensitizer able to trigger the three cell death mechanisms, according to the protocol and cell line [37]. Although not statistically significant, the number of cells undergoing

Fig. 6 MB-PDT phototoxicity could be related to autophagy. **a** Representative images of LC3-puncta immunofluorescence in prostate epithelial tumor cells-PC3 after incubation with 25 μM MB and maintained in the dark (MB) or exposed to low-level laser at 100 J.cm^{-2} energy density (MB-PDT). L group was only irradiated by low-level laser, and the control group was maintained without treatment. **b** Graphical representation of immunofluorescence quantification shows levels of LC3-puncta increased in the MB-PDT group and its reduction after autophagy inhibition by chloroquine (CLQ+ MB-PDT). All values are represented as the means ± SD of three experiments. *$p < 0.05$ compared to control; a=$p < 0.05$ compared to MB-PDT
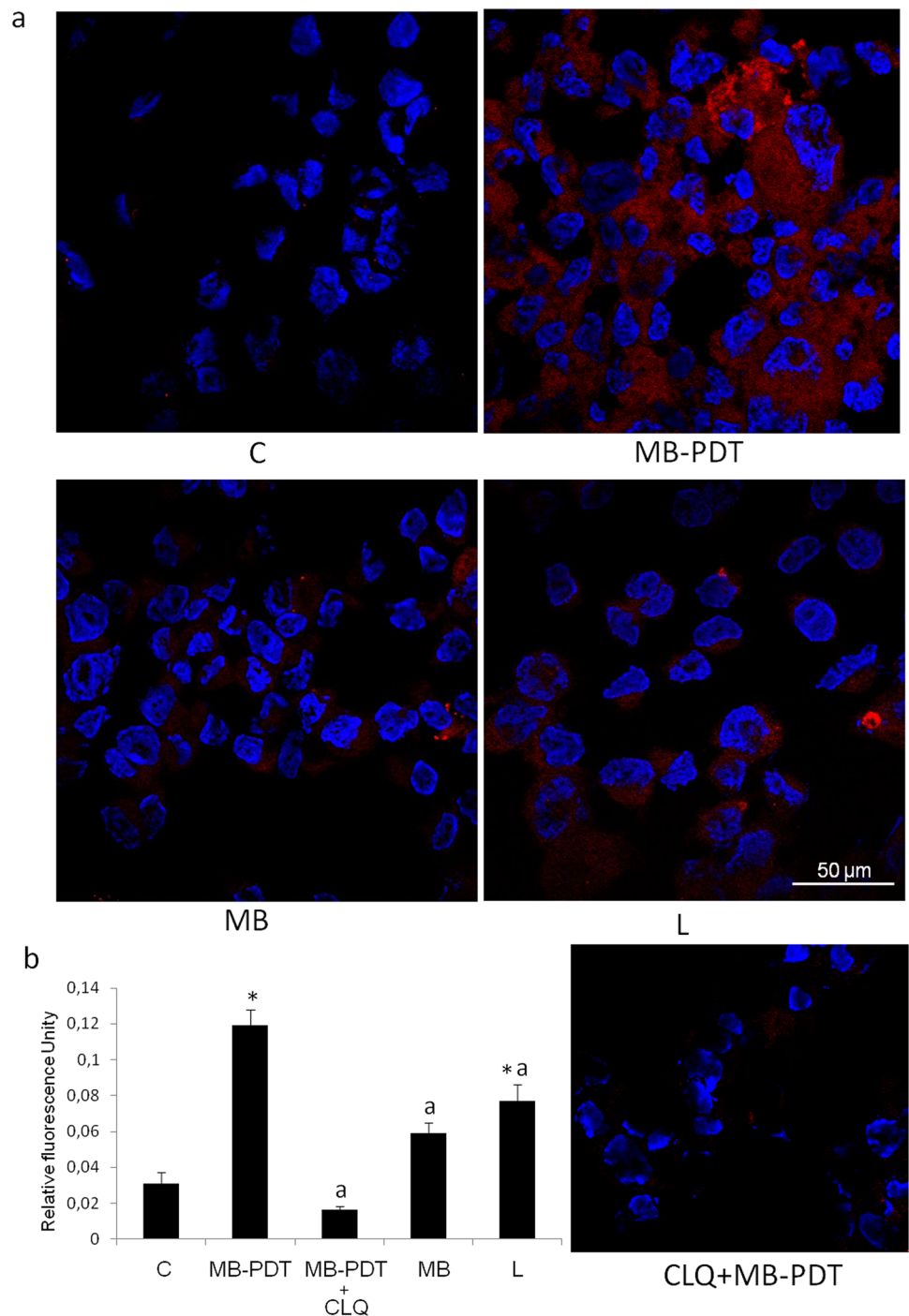
apoptosis was higher in the MB-PDT group than in the control (24 and 15%, respectively). Several studies describe apoptosis as the main type of cell death triggered by PDT. Campos and other authors [38] observed an increase in cytochrome C expression, Fas-L, and BAX/BCL-2 ratio in NIH/3T3 cells submitted to MB-PDT, suggesting an increase in apoptosis. However, Dos Santos and others [29] described the opposite, reporting that caspase inhibition in MCF-7 and MDA-MB-231 cells could not reduce cell death caused by MB-PDT. Our results corroborate with Dos Santos and others [29], showing that caspase-3 activation and apoptosis were not high enough to explain cell viability reduction after MB-PDT. Additionally, such results suggest that, in the short-term MB-PDT, other non-classical pathways of cell death besides apoptosis are likely to be responsible for reduced PC3 cell viability.

Due to this fact, we decided to investigate autophagy, a process that represents a catabolic phenomenon in all
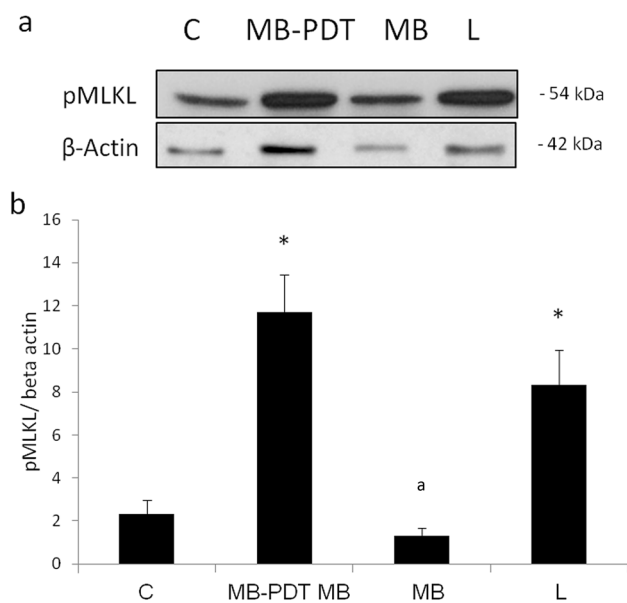
a

b

Fig. 7 Necroptosis is activated by MB-PDT in PC3 cells. Western blotting analysis of phospho-MLKL demonstrated an increase in the activation of this necroptosis molecular marker after MB-PDT treatment. Protein levels from PC3 cells were evaluated after incubation with 25 μM MB (MB) and MB followed by 100 J.cm^{-2} energy density (MB-PDT). L group was only irradiated by low-level laser, and the control group was maintained without treatment. Data of pMLK-L were normalized by β-actin in the same membrane, $n=4$. Each experiment was performed at least three times. *$p<0.05$ versus control group; a$=p<0.05$ versus MB-PDT

eukaryotic cells, important to energy production and cellular homeostasis. Autophagy can have two roles: cell survival or death, depending on cell damage or stress [39, 40]. After autophagy signaling, autophagic vacuole biogenesis begins through the action of the LC3 protein [41]. LC3-I is a protein of diffuse cytoplasmic distribution that, after signaling for autophagy, converts to LC3-II associated with the membrane of the autophagosome [41–43]. This location on autophagosome membranes is known as the "LC3 puncta" pattern, and its quantification, as well as the LC3II/LC3-I ratio, are the most common markers for the study of autophagy [37].

Literature has demonstrated autophagy induction after PDT. Reiners and co-workers [44] observed increased conversion of LC3-I/LC3-II and autophagosomes after mTHPC-PDT in 1c1c7 hepatocytes. Autophagy has also been described in breast tumor cells treated with MB-PDT [29]. LC3-puncta and acridine orange results strongly suggested an increase in autophagy triggered by MB-PDT in PC3 cells. However, interestingly, when the autophagy was blocked with chloroquine, PC3 cell viability was not totally restored. Corroborating with our results, Valli and co-workers [45] also observed such behavior using Pc13-PDT in A375 melanoma cells, describing cell death increase after chloroquine treatment. These authors also showed autophagy

as a mechanism of resistance to PDT and proposed its blockade to increase phototoxicity and potentiate PDT use in anti-cancer therapy. According to Donohoe et al. [37], the presence of autophagosomes is not a definitive indicator that autophagy leads to cell death but a reflex of cell effort to rescue homeostasis and survive in the face of stress. Thus, our data indicate that autophagy may occur as a survival mechanism against the oxidative stress caused by MB-PDT and may stimulate the signaling of other cell death types besides apoptosis.

From these results, we hypothesized a third death pathway that could be involved in reducing the viability of PC3 cells. Necroptosis is a caspase-independent form of regulated cell death, and it has been related to PDT [37]. Goodall and co-workers [46] discovered the necrosome complex colocalization to the autophagosome, and they found that autophagy machinery serves as a scaffold for necrosome complex formation, and ultimately its activation for signaling cell death through necroptosis. Indeed, recent evidence suggests that necroptosis has an essential role in PDT-induced cell death in tumor cells. Liu et al. [47] confirmed that necroptosis is involved in PDT injury in RF/6A cells, which may be MLKL-dependent. Markers for autophagy and necroptosis were found in glioblastoma cells treated with NPe6-PDT [48] and 5-ALA-PDT [49]. Additionally, it has been demonstrated that breast tumor cells also trigger necroptosis in the face of oxidative damage caused by MB-PDT [50]. The present study found elevated levels of MLKL activation after MB-PDT in PC3 cells and based on the knowledge from other studies on necroptosis and PDT, we hypothesized that autophagy might elicit necroptosis in this situation. Our efforts will focus on furthering the knowledge about the effect of MB-PDT on this cell death pathway. Proapoptotic therapy is the principal chemotherapy for cancer treatment, but its effectiveness is limited by drug resistance resulting from disrupted apoptosis machinery [51]. Since necroptosis uses components different from the apoptotic pathway, pro-necroptosis treatments could be an interesting therapy for cancer cell death.

The main feature of PDT is oxidative stress due to ROS production, where cellular components (DNA, proteins, and lipids) are oxidized and damaged. In this regard, PDT causes a collapse of antioxidant systems, leading to cell death. In this investigation, MB-PDT caused oxidative stress in PC3 cells due to decreased levels of catalase and antioxidant potential, and this scenario was associated with increased lipid peroxidation. Lipids are a primary target for oxidative damage in cells, and, indeed, it has been found that cellular membranes are important components of PDT-induced cellular damage for most photosensitizers [52]. As highly reactive compounds, lipid peroxides affect membrane dynamics and can propagate further generation of ROS or degrade into reactive compounds responsible for the cytotoxicity
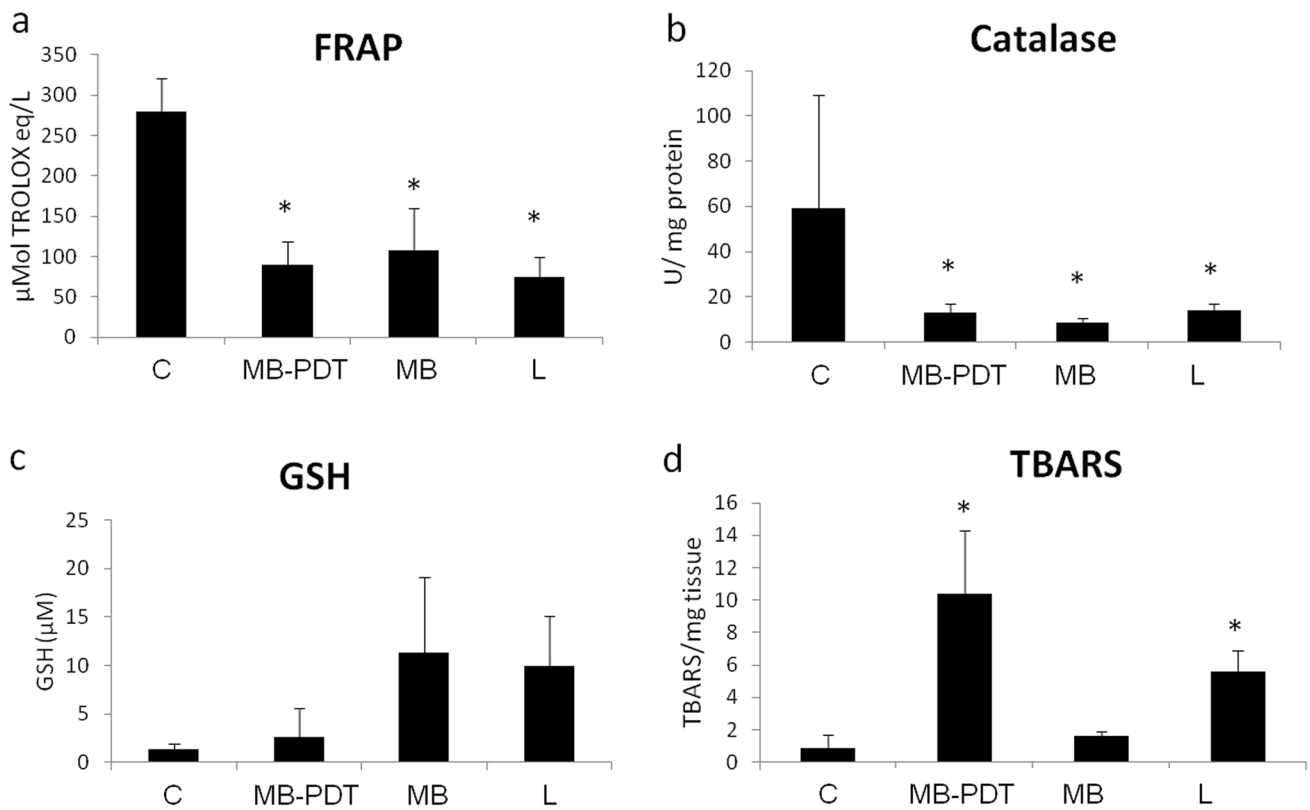
Fig. 8 Analysis of oxidative stress in PC3 after incubation with 25 μM MB (MB) and MB followed by 100 J.cm.$^{-2}$ energy density (MB-PDT). L group was only irradiated by low-level laser, and the control group was maintained without treatment. **a** Total antioxidant activity quantification by FRAP method, which measures Trolox concentration (μMol) showing a reduction in all treated groups; **b** cata-lase activity expressed by micrograms of protein is also decreased by all treatments; **c** GSH content did not change in PC3 cells; and **d** TBARs levels shows an increased lipidic peroxidation in MB-PDT and L group in comparison to control. All values are represented as the means ± SEM of three experiments. *Statistical difference between treated groups and control ($p < 0.05$)

of these molecules [53]. Thus, according to Su et al. [54], the products of lipid peroxidation can stimulate the activation of both the intrinsic and extrinsic apoptotic signaling pathways, as well as trigger autophagy trying to reduce the damage caused by oxidative stress and ferroptosis, a type of programmed cell death [54]. In this regard, dos Santos and cols [50] also have shown that MB-PDT increased lipid peroxidation, and this fenomenum led to ferroptosis in breast tumor cells. Although we have not evaluated ferroptosis, our findings show that the cytotoxic effect of MB-PDT is related to reduced antioxidant potential and oxidative stress in PC3 cells, and this finding could be responsible for triggering autophagy.

In conclusion, MB-PDT treatment reduced the antioxidant potential and increased lipid peroxidation, affecting cell viability and migration in PC3 cells. Such effect was associated with high autophagic activity as a pro-survival response to oxidative damage. Although the increase of apoptosis had been incipient, autophagy could trigger other types of cell death, such as necroptosis, which makes this an efficient cytotoxic treatment for controlling cancer cells. Notably, MB in the concentration used in this investigation presented dark cytotoxicity. An adjustment in dosage and/or exposure time should be considered to improve the efficacy of this treatment.

Availability of data and materials The datasets generated during and/or analyzed during the current study are available from the corresponding author upon reasonable request.

Declarations

Conflicts of interest The authors have no conflict of interest.

Ethical approval For this type of in vitro study, no ethical approval was required.

Consent to participate All authors confirm their participation in this manuscript.

Consent for publication All authors agree to publication.

References

1. Global Health Estimates: Life expectancy and leading causes of death and disability (2019). Accessed on 06 July 2022. Available at: https://www.who.int/data/gho/data/themes/mortality-and-global-health-estimates.
2. Cancer Tomorrow (2018). Accessed on 06 July 2022. Available at: http://gco.iarc.fr/tomorrow/graphic-isotype?type=0&population=900&mode=population&sex=1&cancer=39&age_group=value&apc_male=0&apc_female=0.
3. Fibbi, B., Penna, G., Morelli, A., Adorini, L., & Maggi, M. (2010). Chronic inflammation in the pathogenesis of benign prostatic hyperplasia. *International Journal of Andrology., 33*(3), 475–488. https://doi.org/10.1111/j.1365-2605.2009.00972.x
4. Ho, E., Boileau, T. W. M., & Bray, T. M. (2004). Dietary influences on endocrine–inflammatory interactions in prostate cancer development. *Archives of Biochemistry and Biophysics., 428*(1), 109–117. https://doi.org/10.1016/j.abb.2004.01.009
5. Leitzmann, M. F., & Rohrmann, S. (2012). Risk factors for the onset of prostatic cancer: age, location, and behavioral correlates. *Clinical Epidemiology, 4*, 1–11. https://doi.org/10.2147/CLEP.S16747
6. Martins, W. K., Belotto, R., Silva, M. N., Grasso, D., Suriani, M. D., Lavor, T. S., Itri, R., Baptista, M. S., & Tsubone, T. M. (2021). Autophagy regulation and photodynamic therapy: insights to improve outcomes of cancer treatment. *Frontiers in Oncology., 10*, 610472. https://doi.org/10.3389/fonc.2020.610472
7. Dolmans, D. E., Fukumura, D., & Jain, R. K. (2003). Photodynamic therapy for cancer. *Nature Reviews Cancer, 3*(5), 380–387. https://doi.org/10.1038/nrc1071
8. Lim, D. J. (2021). Methylene blue-based nano and microparticles: fabrication and applications in photodynamic therapy. *Polymers, 13*, 3955. https://doi.org/10.3390/polym13223955
9. Franchi, L. P., de Freitas Lima, J. E. B., Piva, H. L., & Tedesco, A. C. (2020). The redox function of apurinic/apyrimidinic endo-nuclease 1 as a key modulator in photodynamic therapy. *Journal of Photochemistry and Photobiology B: Biology., 211*, 111992. https://doi.org/10.1016/j.jphotobiol.2020.111992
10. Orth, K., Beck, G., Genze, F., & Rück, A. (2000). Methylene blue mediated photodynamic therapy in experimental colorectal tumors in mice. *Journal of Photochemistry and Photobiology, B: Biology, 57*(2–3), 186–192. https://doi.org/10.1016/s1011-1344(00)00105-6
11. Petrellis, M. C., Frigo, L., Ribeiro, W., Leal-Junior, E. C., Oliveira, F. R., Maria, D. A., & Lopes-Martins, R. Á. (2019). Proinflammatory effects of photoactivated methylene blue on rat

12. model of Walker 256 carcinosarcoma. *Experimental Oncology., 41*(2), 112–122.
13. Tardivo, J. P., Giglio, A., Oliveira, C. S., Gabrielli, D. S., Junqueira, H. C., Tada, D. B., Severino, D., Turchiello, R. F., & Baptista, M. S. (2005). Methylene blue in photodynamic therapy: from basic mechanisms to clinical applications. *Photodiagnosis And Photodynamic Therapy., 2*(3), 175–191.
14. Bojadzic, D., Alcazar, O., & Buchwald, P. (2021). Methylene blue inhibits the SARS-CoV-2 spike—ACE2 protein-protein interaction—a mechanism that can contribute to its antiviral activity against COVID-19. *Frontiers in Pharmacology, 11*, 2255. https://doi.org/10.3389/fphar.2020.600372
15. Fan, Z., Dai, X., Lu, Y., Yu, E., Brahmbatt, N., Carter, N., & Ray, P. A. (2014). Enhancing targeted tumor treatment by near IR light-activatable photodynamic–photothermal synergistic therapy. *Molecular Pharmaceutics, 11*(4), 1109–1116. https://doi.org/10.1021/mp4002816
16. Fahey, J. M., & Girotti, A. W. (2015). Accelerated migration and invasion of prostate cancer cells after a photodynamic therapy-like challenge: Role of nitric oxide. *Nitric Oxide, 49*, 47–55. https://doi.org/10.1016/j.niox.2015.05.006
17. Hayashida, Y., Ikeda, Y., Sawada, K., Kawai, K., Kato, T., Kakehi, Y., & Araki, N. (2016). Invention of a novel photodynamic therapy for tumors using a photosensitizing PI3K inhibitor. *International Journal of Cancer, 139*(3), 700–711. https://doi.org/10.1002/ijc.30097
18. Kawczyk-Krupka, A., Wawrzyniec, K., Musiol, S. K., Potempa, M., Bugaj, A. M., & Sieroń, A. (2015). Treatment of localized prostate cancer using WST-09 and WST-11 mediated vascular targeted photodynamic therapy—a review. *Photodiagnosis and Photodynamic Therapy., 12*(4), 567–574. https://doi.org/10.1016/j.pdpdt.2015.10.001
19. Gebäck, T., Schulz, M. M. P., Koumoutsakos, P., & Detmar, M. (2009). TScratch: a novel and simple software tool for automated analysis of monolayer wound healing assays: short technical reports. *BioTechniques, 46*(4), 265–274. https://doi.org/10.2144/000113083
20. Hartig, S. M. (2013). Basic image analysis and manipulation in ImageJ. *Current Protocols in Molecular Biology, 102*(1), 14–15. https://doi.org/10.1002/0471142727.mb1415s102
21. Paglin, S., Hollister, T., Delohery, T., Hackett, N., McMahill, M., Sphicas, E., & Yahalom, J. (2001). A novel response of cancer cells to radiation involves autophagy and formation of acidic vesicles. *Cancer Research, 61*(2), 439–444.
22. Bradford, M. M. (1976). A rapid and sensitive method for the quantitation of microgram quantities of protein utilizing the principle of protein-dye binding. *Analytical Biochemistry, 72*(1–2), 248–254. https://doi.org/10.1006/abio.1976.9999
23. Aebi, H. (1984). Catalase in vitro In Methods in enzymology. *Academic Press, 105*, 121–126. https://doi.org/10.1016/s0076-6879(84)05016-3
24. Benzie, I. F., & Strain, J. J. (1996). The ferric reducing ability of plasma (FRAP) as a measure of "antioxidant power": the FRAP assay. *Analytical Biochemistry, 239*(1), 70–76. https://doi.org/10.1006/abio.1996.0292
25. Draper, H. H., & Hadley, M. (1990). Malondialdehyde determination as index of lipid Peroxidation In Methods in enzymology. *Academic Press, 186*, 421–431. https://doi.org/10.1016/0076-6879(90)86135-i
26. Akerboom, T. P., & Sies, H. (1981). Assay of glutathione, glutathione disulfide, and glutathione mixed disulfides in biological samples In Methods in enzymology. *Academic Press, 77*, 373–382. https://doi.org/10.1016/s0076-6879(81)77050-2
27. Allegra, A., Pioggia, G., Tonacci, A., Musolino, C., & Gangemi, S. (2020). Oxidative stress and photodynamic therapy of skin

cancers: Mechanisms, challenges and promising developments. *Antioxidants, 9*(5), 448. https://doi.org/10.3390/antiox9050448

27. Wainwright, M., & Crossley, K. B. (2002). Methylene blue-a therapeutic dye for all seasons? *Journal of Chemotherapy, 14*(5), 431–443. https://doi.org/10.1179/joc.2002.14.5.431

28. Bellin, J. S., Mohos, S. C., & Oster, G. (1961). Dye-sensitized photoinactivation of tumor cells in vitro. *Cancer Research, 21*(10), 1365–1371.

29. Dos Santos, A. F., Terra, L. F., Wailemann, R. A., Oliveira, T. C., Gomes, V. D. M., Mineiro, M. F., & Labriola, L. (2017). Methylene blue photodynamic therapy induces selective and massive cell death in human breast cancer cells. *BMC Cancer, 17*(1), 1–15. https://doi.org/10.1186/s12885-017-3179-7

30. Monroe, J. D., Belekov, E., Er, A. O., & Smith, M. E. (2019). Anticancer photodynamic therapy properties of sulfur-doped graphene quantum dot and methylene blue preparations in MCF-7 breast cancer cell culture. *Photochemistry and Photobiology, 95*(6), 1473–1481. https://doi.org/10.1111/php.13136

31. Lim, E. J., Oak, C. H., Heo, J., & Kim, Y. H. (2013). Methylene blue-mediated photodynamic therapy enhances apoptosis in lung cancer cells. *Oncology Reports, 30*(2), 856–862. https://doi.org/10.3892/or.2013.2494

32. Lu, Y., Jiao, R., Chen, X., Zhong, J., Ji, J., & Shen, P. (2008). Methylene blue-mediated photodynamic therapy induces mitochondria-dependent apoptosis in hela cell. *Journal of Cellular Biochemistry, 105*(6), 1451–1460. https://doi.org/10.1002/jcb.21965

33. Jiang, C., Yang, W., Wang, C., Qin, W., Ming, J., Zhang, M., Qian, H., & Jiao, T. (2019). Methylene blue-mediated photodynamic therapy induces macrophage apoptosis via ROS and reduces bone resorption in periodontitis. *Oxidative Medicine and Cellular Longevity, 2019*, 1529520. https://doi.org/10.1155/2019/1529520

34. Khanal, A., Bui, M. P. N., & Seo, S. S. (2014). Microgel-encapsulated methylene blue for the treatment of breast cancer cells by photodynamic therapy. *Journal of Breast Cancer, 17*(1), 18–24. https://doi.org/10.4048/jbc.2014.17.1.18

35. Ma, M., Cheng, L., Zhao, A., Zhang, H., & Zhang, A. (2020). Pluronic-based graphene oxide-methylene blue nanocomposite for photodynamic/photothermal combined therapy of cancer cells. *Photodiagnosis Photodyn., 29*, 101640. https://doi.org/10.1016/j.pdpdt.2019.101640

36. Bacac, M., & Stamenkovic, I. (2008). Metastatic cancer cell. *Annual Review of Pathology: Mechanisms of Disease, 3*, 221–247. https://doi.org/10.1146/annurev.pathmechdis.3.121806.151523

37. Donohoe, C., Senge, M. O., Arnaut, L. G., & Gomes-da-Silva LC (2019) Cell death in photodynamic therapy: From oxidative stress to anti-tumor immunity. *Biochimica et Biophysica Acta (BBA) Reviews on Cancer, 2*, 188308. https://doi.org/10.1016/j.bbcan.2019.07.003

38. Lamarque, G. C. C., Méndez, D. A. C., Matos, A. A., Dionisio, T. J., Machado, M. A. A. M., Magalhaes, A. C., & Cruvinel, T. (2020). Cytotoxic effect and apoptosis pathways activated by methylene blue-mediated photodynamic therapy in fibroblasts. *Photodiagnosis and Photodynamic Therapy., 29*, 101654. https://doi.org/10.1016/j.pdpdt.2020.101654

39. Duprez, L., Wirawan, E., Berghe, T. V., & Vandenabeele, P. (2009). Major cell death pathways at a glance. *Microbes and Infection, 11*(13), 1050–1062. https://doi.org/10.1016/j.micinf.2009.08.013

40. Elmore, S. (2007). Apoptosis: a review of programmed cell death. *Toxicologic Pathology, 35*(4), 495–516. https://doi.org/10.1080/01926230701320337

41. Gallagher, L. E., Williamson, L. E., & Chan, E. Y. (2016). Advances in autophagy regulatory mechanisms. *Cells, 5*(2), 24. https://doi.org/10.3390/cells5020024

42. Martins, W. K., Belotto, R., Silva, M. N., Grasso, D., Suriani, M. D., Lavor, T. S., & Tsubone, T. M. (2021). Autophagy regulation and photodynamic therapy: insights to improve outcomes of cancer treatment. *Frontiers in Oncology., 10*, 610472. https://doi.org/10.3389/fonc.2020.610472

43. Mizushima, N. (2007). Autophagy: Process and function. *Genes & Development, 21*(22), 2861–2873. https://doi.org/10.1101/gad.1599207

44. Reiners, J. J., Agostinis, P., Berg, K., Oleinick, N. L., & Kessel, D. H. (2010). Assessing autophagy in the context of photodynamic therapy. *Autophagy, 6*(1), 7–18. https://doi.org/10.4161/auto.6.1.10220

45. Valli, F., Vior, M. C. G., Roguin, L. P., & Marino, J. (2020). Crosstalk between oxidative stress-induced apoptotic and autophagic signaling pathways in Zn (II) phthalocyanine photodynamic therapy of melanoma. *Free Radical Biology & Medicine, 152*, 743–754. https://doi.org/10.1016/j.freeradbiomed.2020.01.018

46. Goodall, M. L., Cramer, S. D., & Thorburn, A. (2016). Autophagy complexes cell death by necroptosis. *Oncotarget, 7*(32), 50818.

47. Liu, Y., Zhu, M., Gong, R., Wang, X., Li, L., & Xu, G. (2020). Pre-treatment With ranibizumab aggravates PDT injury and alleviates inflammatory response in choroid-retinal endothelial cells. *Frontiers in Cell and Developmental Biology., 8*, 608. https://doi.org/10.3389/fcell.2020.00608

48. Miki, Y., Akimoto, J., Moritake, K., Hironaka, C., & Fujiwara, Y. (2015). Photodynamic therapy using talaporfin sodium induces concentration-dependent programmed necrosis in human glioblastoma T98G cells. *Lasers in Medical Science, 30*(6), 1739–1745. https://doi.org/10.1007/s10103-015-1783-9

49. Fettweis, G., Di Valentin, E., L'homme, L., Lassence, C., Dequiedt, F., Fille, M., Coupienne, I., & Piette, J. (1864). (2017) RIP3 antagonizes a TSC2-mediated pro-survival pathway in glioblastoma cell death Biochim Biophys. *Biochimica et Biophysica Acta (BBA) Molecular Cell Research., 1*, 113–124. https://doi.org/10.1016/j.bbamcr.2016.10.014

50. Dos Santos, A. F., Inague, A., Arini, G. S., Terra, L. F., Wailemann, R. A., Pimentel, A. C., Yoshinaga, M. Y., Silva, R. R., Severino, D., Almeida, D. R. Q., Gomes, V. M., Cardoso, A. B., Tera, W. R., Miyamoto, S., Baptista, M. S., & Labriola, L. (2020). Distinct photo-oxidation-induced cell death pathways lead to selective killing of human breast cancer cells. *Cell Death & Disease, 11*(12), 1–12. https://doi.org/10.1038/s41419-020-03275-2

51. Su, Z., Yang, Z., Xie, L., DeWitt, J. P., & Chen, Y. (2016). Cancer therapy in the necroptosis era. *Cell Death and Differentiation, 23*(5), 748–756. https://doi.org/10.1038/cdd.2016.8

52. Itri, R., Junqueira, H. C., Mertins, O., & Baptista, M. S. (2014). Membrane changes under oxidative stress: The impact of oxidized lipids. *Biophysical Reviews, 6*(1), 47–61. https://doi.org/10.1007/s12551-013-0128-9

53. Gaschler, M. M., & Stockwell, B. R. (2017). Lipid peroxidation in cell death. *Biochemical and Biophysical Research Communications, 482*(3), 419–425. https://doi.org/10.1016/j.bbrc.2016.10.086

54. Su, L. J., Zhang, J. H., Gomez, H., Murugan, R., Hong, X., Xu, D., & Peng, Z. Y. (2019). Reactive oxygen species-induced lipid peroxidation in apoptosis, autophagy, and ferroptosis. *Oxidative Medicine and Cellular Longevity, 2019*, 5080843. https://doi.org/10.1016/j.bbrc.2016.10.086

Authors and Affiliations

Laura Calazans de Melo Gomes[1] · Amanda Branquinho de Oliveira Cunha[1] · Luiz Felipe Fernandes Peixoto[1] · Renata Graciele Zanon[2] · Françoise Vasconcelos Botelho[3] · Marcelo José Barbosa Silva[4] · Maria Etelvina Pinto-Fochi[5] · Rejane Maira Góes[6] · Flávia de Paoli[7] · Daniele Lisboa Ribeiro[1]

✉ Daniele Lisboa Ribeiro
daniele.ribeiro@ufu.br

[1] Department of Cell Biology, Histology and Embryology. Institute of Biomedical Sciences-ICBIM, Federal University of Uberlândia-UFU, Uberlândia, Minas Gerais, Brazil

[2] Department of Anatomy. Institute of Biomedical Sciences-ICBIM, Federal University of Uberlândia-UFU, Uberlândia, Minas Gerais, Brazil

[3] Institute of Biotechnology-IBTEC, Federal University of Uberlândia-UFU, Uberlândia, Minas Gerais, Brazil

[4] Department of Immunology, Institute of Biomedical Sciences-ICBIM, Federal University of Uberlândia-UFU, Uberlândia, Minas Gerais, Brazil

[5] Faculdade de Medicina, União das Faculdades Dos Grandes Lagos, São José Do Rio Preto-São Paulo, São Paulo, Brazil

[6] Department of Biology, Institute of Biosciences, Humanities and Exact Sciences, São Paulo State University-UNESP, São José Do Rio Preto-São Paulo, Brazil

[7] Department of Morphology, Institute of Biological Sciences, Federal University of Juiz de Fora-UFJF, Juiz de Fora, Minas Gerais, Brazil